Incorporation of A_2Q into HgQ and Dimensional Reduction to $A_2Hg_3Q_4$ and $A_2Hg_6Q_7$ (A = K, Rb, Cs; Q = S, Se). Access of Li Ions in $A_2Hg_6Q_7$ through Topotactic Ion-Exchange

Enos A. Axtell, III, Younbong Park, Konstantinos Chondroudis, and Mercouri G. Kanatzidis*

Contribution from the Department of Chemistry and Center for Fundamental Materials Research, Michigan State University, East Lansing, Michigan 48824-1322

Received April 28, 1997[⊗]

Abstract: The synthesis of the one-dimensional $K_2Hg_3Q_4$ (Q = S, Se) and $Cs_2Hg_3Se_4$ and the three-dimensional $A_2Hg_6S_7$ (A = K, Rb, Cs), and $A_2Hg_6Se_7$ (A = Rb, Cs) in reactive A_2Q_x fluxes is reported. Pale yellow, hexagonal plates of $K_2Hg_3S_4$ crystallize in space group *Pbcn*, with $a = 10.561(5)$ Å, $b = 6.534(3)$ Å, and $c = 13.706(2)$ Å, $V = 945.8(7)$ Å,^{3} $d_{calc} = 5.68$ g/cm^3, and final $R = 5.7\%$, $R_w = 6.3\%$. Red, hexagonal plates of $K_2Hg_3Se_4$ crystallize in space group *Pbcn*, with $a = 10.820(2)$ Å, $b = 6.783(1)$ Å, and $c = 14.042(2)$ Å, $V = 1030.6(5)$ Å,^{3} $d_{calc} = 6.42$ g/cm^3, and final $R = 7.7\%$, $R_w = 8.4\%$. Orange yellow, hexagonal plates of $Cs_2Hg_3Se_4$ crystallize in space group *Pbcn*, with $a = 12.047(4)$ Å, $b = 6.465(2)$ Å, and $c = 14.771(6)$ Å, $V = 1150.4(7)$ Å,^{3} $d_{calc} = 6.83$ g/cm^3, and final $R = 5.5\%$, $R_w = 6.2\%$. Black needles of $K_2Hg_6S_7$ crystallize in space group $P\bar{4}2_1m$, with $a = 13.805(8)$ Å and $c = 4.080(3)$ Å, $V = 778(1)$ Å,^{3} $d_{calc} = 6.43$ g/cm^3, and final $R = 3.1\%$, $R_w = 3.6\%$. Black needles of $Rb_2Hg_6S_7$ crystallize in space group $P4_2nm$, with $a = 13.9221(8)$ Å and $c = 4.1204(2)$ Å, $V = 798.6(1)$ Å,^{3} $d_{calc} = 6.65$ g/cm^3, and final $R = 4.3\%$, $R_w = 5.0\%$. Black needles of $Cs_2Hg_6S_7$ crystallize in space group $P4_2nm$, with $a = 13.958(4)$ Å and $c = 4.159(2)$ Å, $V = 810.2(8)$ Å,^{3} $d_{calc} = 6.94$ g/cm^3, and final $R = 4.3\%$, $R_w = 4.4\%$. Black needles of $Cs_2Hg_6Se_7$ crystallize in space group $P4_2nm$, with $a = 14.505(7)$ Å and $c = 4.308(2)$ Å, $V = 906(1)$ Å,^{3} $d_{calc} = 7.41$ g/cm^3, and final $R = 3.6\%$, $R_w = 4.0\%$. The $A_2Hg_3Q_4$ compounds contain linear chains. The $A_2Hg_6Q_7$ compounds display noncentrosymmetric frameworks with A^+ cations residing in tunnels formed by both tetrahedral and linear Hg atoms. $K_2Hg_6S_7$, $Rb_2Hg_6S_7$, $Cs_2Hg_6S_7$, $Rb_2Hg_6Se_7$, and $Cs_2Hg_6Se_7$ display room-temperature bandgaps of 1.51, 1.55, 1.61, 1.13, and 1.17 eV, respectively. Bandgap engineering through S/Se solid solutions of the type $Rb_2Hg_6Se_{7-x}S_x$ and $Cs_2Hg_6Se_{7-x}S_x$ is possible in these materials. All $A_2Hg_6Q_7$ melt congruently, with melting points of 556 ± 10 °C, except for $Rb_2Hg_6Se_7$ which degrades. $Rb_2Hg_6S_7$ can undergo ion exchange reactions with LiI to give $Li_{1.8}Rb_{0.2}Hg_6S_7$.

Introduction

The utility of alkali metal polychalcogenide fluxes as solvents and reagents at intermediate temperatures has been amply noted.[1] An enormous number of interesting new compounds with low-dimensional structures occur at these temperatures (150∼500 °C). Solid-state chalcogenides are of great interest due to their useful electronic[2] and catalytic[3] properties. For example, the chalcogenides with zinc blende or chalcopyrite structure such as $CuInSe_2$, CdTe, and $Hg_{1-x}Cd_xTe$ find applications in photovoltaic devices for solar energy conversion and infrared detection, respectively.[4] From a chemical point of view it would be interesting to see how the insertion of alkali chalcogenide equivalents into such three-dimensional structures affects the structural organization of the resulting metal−chalcogenide framework, particularly in terms of dimensionality and how the latter correlates with observed properties. In this context, recently we have demonstrated the ability of the molten salt method to generate "break-up" or low-dimensional structures such as $K_2Cd_2S_3$,[5] $K_2Cd_3S_4$,[6] $K_2Cd_3Se_4$,[6] $Rb_2Cd_3Se_4$,[6] and $K_2Cd_3Te_4$.[7] These compounds, whose Cd/Q connectivity is reduced relative to that of the parent CdQ structure, display bandgaps that range from 0.31 to 0.76 eV higher than the CdQ

[⊗] Abstract published in *Advance ACS Abstracts,* December 15, 1997.

(1) (a) Kanatzidis, M. G. *Chem. Mater*. **1990**, *2*, 353−363. (b) Kanatzidis, M. G.; Sutorik, A. C. *Prog. Inorg. Chem.* **1995**, *43*, 151−265.

(2) (a) Meerschaut, A.; Rouxel, J. In *Crystal Chemistry and Properties of Materials with Quasi One-Dimensional Structures*; Rouxel, J., Ed.; D. Reidel Publishing Co.: **1986**, 205−279. (b) *Superconductivity in Ternary Compounds*; Bischer, O., Maple, M. B., Eds., Springer: Berlin, **1982**; Vols I and II. (c) Chevral, R. In *Superconductor Materials Science: Metallurgy, Fabrication and Applications*; Foner, S.; Schwart, B. B., Eds.; Plenum Press: New York, 1981, Chapter 10. d) Whittingham, M. S. *Prog. Solid State Chem*. **1978**, *12*, 41−99.

(3) (a) Alonso-Vante, N.; Jaejermann, W.; Tributch, H.; Hönle, W.; Yvon, K. *J. Am. Chem. Soc*. **1987**, *111*, 3251−3257. (b) Weisser, O.; Landa, S. *Sulfide Catalysis: Their Properties and Applications*; Pergammon: London, 1973. (c) Chianelli, R. R.; Pecoraro, T. A.; Halbert, T. R.; Pan, W−H.; Stiefel, E. I. *J. Catal*. **1984**, *86*, 226−230. (d) Pecoraro, T. A.; Chianelli, R. R. *J. Catal*. **1981**, *67*, 430−445.

(4) (a) Zweibel, K.; Michell, R. *CuInSe$_2$ and CdTe: Scale-up for Manufacturing*; Solar Energy Research Institute, Dec 1989, and references therein. (b) Mickelsen, R. A.; Chen, W. S. In *Ternary and Multinary Compounds*; Deb, S. K., Zunger, Z., Eds.; Proceedings of the 7th Conference, Materials Research Society, 1987; pp 39−47. (c) Steward, J. M.; Chen, W. S.; Devaney, W. E.; Mickelsen, R. A. In *Ternary and Multinary Compounds*; Deb, S. K., Zunger, Z., Eds.; Proceedings of the 7th Conference, Materials Research Society, 1987; pp 59−64.

(5) Axtell, E. A.; Liao, J−H.; Pikramenou, Z.; Park, Y.; Kanatzidis, M. G. *J. Am. Chem. Soc.* **1993**, *115*, 12191−2.

(6) Axtell, E. A.; Liao, J−H.; Pikramenou, Z.; Kanatzidis, M. G. *Chem. Eur. J.* **1996**, *2*, 656−666.

(7) Axtell, E. A. Ph.D. Dissertation, Michigan State University, 1995.

S0002-7863(97)01348-6 CCC: $15.00
Published on Web 01/14/1998

binaries. An interesting illustration of dimensional reduction has been recently shown in the Cat/Re_6S_8/X system where Cat is a counterion and X is a halide.[8]

Dimensional reduction can be exploited to generate materials with desired bandgaps from corresponding binary compounds with smaller bandgaps. For example, the cubic forms of HgS and HgSe have bandgaps with $E_g \sim 0.0$ eV and are two possible candidates from which to generate new "break-up" structures with higher bandgaps. This would result in ternary A/Hg/Q type compounds (A = alkali metal) of which few are known. These include A_6HgQ_4 (A = K, Rb; Q = S, Se),[9a] Na_2HgS_2, [9b] K_2HgS_2,[9b] $Na_2Hg_3S_4$,[10] $Na_2Hg_6S_7 \cdot H_2O$,[11] and $Rb_2Hg_3Te_4$.[12] We focused our investigation of ternary A_2Q/HgQ systems on the alkali metal polychalcogenide fluxes (A_2Q_x) at intermediate temperatures. In this contribution, we report a full account of the preparation and properties of a family of new ternary homologous compounds, $A_2Hg_3Q_4$ (A = K, Cs; Q = S, Se) and $A_2Hg_6Q_7$ (A = K, Rb, Cs; Q = S, Se), which feature mixed mercury coordination and unusual low-dimensional structure types. These materials and their properties are discussed in the context of dimensional reduction of the parent compound HgQ brought about by the incorporation into it of A_2Q equivalents. Of these, $K_2Hg_3S_4$ and $K_2Hg_6S_7$ have been reported in preliminary form.[13] We demonstrate that the tunneled framework in $A_2Hg_6Q_7$ can act as a host structure by undergoing topotatcic ion-exchange reactions with LiI.

Experimental Section

Materials. Chemicals in this work were used as obtained: mercury sulfide (HgS) powder, analytical reagent, J. T. Baker Chemical Co., Phillipsburg, NJ; mercury selenide (HgSe) powder, −100 mesh, 99.9% purity, Cerac, Milwaukee, WI; sulfur powder, Spectrum Chemical Mfg. Corp. (Lot No. EE597); selenium powder, −100 mesh, 99.95% purity, Aldrich Chemical Co., Milwaukee, WI; potassium metal (98%), Aldrich Chemical Co., Milwaukee, WI; rubidium metal, Cerac; and cesium metal, 99.98% purity, AESAR, Johnson Matthey, Seabrook, NH.

Synthesis. (a) K_2S. Potassium sulfide was produced in liquid ammonia. In a nitrogen-filled glovebox, the stoichiometric amounts of potassium metal chunks and sulfur powder necessary to produce 20 g of starting material were loaded into a 250 mL round-bottom flask. A Teflon stir bar was added and the flask closed to air with a glass adapter and valve. This apparatus was removed to a Schlenk line, where approximately 150 mL of liquid ammonia was condensed under nitrogen, with stirring, into the dry ice/acetone cooled round-bottom flask. After the flask was allowed to warm to room temperature, the apparatus was put under vacuum for several hours, followed by heating with a hot air gun to drive off any remaining ammonia. The apparatus was returned to the glovebox, and the product was ground to a fine powder before use. The powder was pale yellow in color.

(b) Rb_2S, Cs_2S, Rb_2Se, and Cs_2Se. In a nitrogen filled glovebox, rubidium or cesium metal was gently heated until molten. Approximately 10 g of the alkali metal was subsequently weighed into a three-necked, 500-mL round-bottom flask. The center neck was closed with a glass adapter and valve, while the two outer necks were closed with ground glass stoppers. The apparatus was then moved to a Schlenk line. Liquid ammonia was condensed, under nitrogen, into the dry ice/acetone-cooled round-bottom flask. After the flask was filled half full and swirled to dissolve the alkali metal, a Teflon-coated stir bar was added through a side neck. The stoichiometric amount of elemental sulfur or selenium needed was added with stirring. Subsequently, the material was treated as above, resulting in a pale yellow or orange powder for the sulfides and the selenides, respectively. **Caution:** Alkali metals are highly reactive! The flask residue was rinsed carefully with isopropyl alcohol to destroy any remaining alkali metal.

(c) HgSe. HgSe was prepared by pipeting approximately 1.0 g of liquid mercury into a 9 mm o.d. × 7 mm i.d. fused silica tube and then adding the stoichiometric amount of elemental selenium. The tube was sealed under a dynamic vacuum of 2.0×10^{-4} mbar and placed in a computer-controlled furnace. The furnace was heated to 700 °C over 48 h, held at isotherm for 12 h, then cooled at 20 °C/h to 50 °C. The ingot was removed from the tube and ground to a powder before use. **Caution:** Liquid mercury is volatile and toxic! The temperature was raised slowly to allow the mercury to react without evaporating. Ideally, the reaction should be run in a fume hood.

(d) $K_2Hg_3S_4$ (I). 0.165 g (1.5 mmol) amount of K_2S, 0.116 g (0.5 mmol) of HgS, and 0.128 g (4.0 mmol) of S were mixed together and loaded in a Pyrex tube that was then flame-sealed under vacuum ($\sim 10^{-3}$ mbar). The tube was placed in a computer-controlled furnace and heated at 220 °C for 99 h, then cooled slowly to 50 °C at a rate of 2 °C/h. Pale yellow transparent hexagonal shaped crystals were obtained with a small contamination of HgS by removing excess potassium polysulfides with degassed dimethylformamide (DMF) under a N_2 atmosphere. A yield of 46%, based on HgS, is typical. The product is not stable in water and decomposes rapidly. The presence of K, Hg, and S atoms in a large number of crystals was confirmed by using the EDS/SEM system.

(e) $K_2Hg_3Se_4$ (II). A of 0.118 g (1.75 mmol) amount of K_2Se, 0.070 g (0.25 mmol) of HgSe, and 0.158 g (2.0 mmol) of Se were mixed together and loaded in a Pyrex tube that was then flame-sealed under vacuum ($\sim 10^{-3}$ mbar). The tube was placed in a computer-controlled furnace and heated at 250 °C for 99 h, then cooled slowly to 50 °C at a rate of 2 °C/h Red hexagonal shaped crystals were obtained with a small contamination of HgSe by removing excess potassium polyselenides with degassed DMF under a N_2 atmosphere. A yield of 53%, based on HgSe, is typical. The product is not stable in water and decomposes rapidly.

(f) $Cs_2Hg_3Se_4$ (III). A 0.115 g (0.33 mmol) amount of Cs_2Se, 0.047 g (0.17 mmol) of HgSe, and 0.105 g (1.33 mmol) of Se were mixed together and loaded in a Pyrex tube that was then flame-sealed under vacuum ($\sim 10^{-3}$ mbar). The tube was placed in a computer-controlled furnace and heated at 250 °C for 99 h, then cooled slowly to 50 °C at a rate of 2 °C/h Orange-yellow hexagonal shaped crystals were obtained, with a small contamination of HgSe, by removing excess cesium polyselenides with degassed DMF under a N_2 atmosphere. A yield of 58%, based on HgSe, is typical. The product is relatively stable in water for a short period of time, but decomposes in an hour. A quantitative microprobe analysis performed on a large number of crystals with an EDS/SEM microanalysis system gave an average composition of $Cs_{1.9}Hg_{3.0}Se_{3.8}$.

(g) $K_2Hg_6S_7$ (IV). A 0.055 g (0.5 mmol) amount of K_2S, 0.203 g (0.87 mmol) of HgS, and 0.064 g (2.0 mmol) of S were mixed together and loaded in a Pyrex tube that was then flame-sealed under vacuum ($\sim 10^{-3}$ mbar). The tube was placed in a computer-controlled furnace and heated at 370 °C for 99 h, then cooled slowly to 50 °C at a rate of 2 °C/h. Black needlelike crystals were obtained, with little contamination of red HgS crystals, by removing excess molten potassium polysulfides with water under a N_2 atmosphere. A yield of 72%, based on HgS, is typical. The product was washed with ethanol and ether and vacuum dried. The product is insoluble in water and common organic solvents. A quantitative microprobe analysis performed on a large number of crystals with the EDS/SEM system gave an average composition of $K_{2.0}Hg_{5.8}S_{7.1}$.

This compound can also be prepared by direct synthesis: 0.110 g (1.0 mmol) of K_2S and 1.396 g (6 mmol) of HgS were mixed together and loaded in a Pyrex tube that was then flame-sealed under vacuum ($\sim 10^{-3}$ mbar). The tube was placed in a computer-controlled furnace and heated at 375 °C for 7 days and cooled slowly to 50 °C at a rate of 2 °C/h. A black powder of $K_2Hg_6S_7$ was obtained with little

(8) Long, J. R.; McCarty, L. S.; Holm, R. H. *J. Am. Chem. Soc.* **1996**, *118*, 4603−4616.
(9) (a) Sommer, H.; Hoppe, R. *Z. Anorg. Allg. Chem.* **1978**, *443*, 201−211. (b) Klepp, K. O.; Prager, K. *Z. Naturforsch.* **1992**, *47B*, 491−496.
(10) Klepp, K. O. *J. Alloys Compds.* **1992**, *182*, 281−288.
(11) Herath Banda, R. M.; Craig, D.; Dance, I. G.; Scudder M. *Polyhedron* **1991**, *10*, 41−45.
(12) Li, J.; Chen, Z.; Lam, K−C.; Mulley, S.; Proserpio, D. M. *Inorg. Chem.* **1997**, *36*, 684−687.
(13) Kanatzidis, M. G.; Park, Y. *Chem. Mater.* **1990**, *2*, 99−101.

contamination of red HgS and was identified by its X-ray powder diffraction pattern.

(h) $Rb_2Hg_6S_7$ (V). Black needles of $Rb_2Hg_6S_7$ were obtained in bulk amounts by the reaction of 1.486 g (7.3 mmol) of Rb_2S and 10.221 g (44 mmol) of HgS. This charge was sealed inside an evacuated quartz tube. The tube was placed inside a computer-controlled furnace and heated at 400 °C for 1.5 days, followed by heating at 500 °C for 1 day, slow cooling to 415 °C, and quenching to room temperature. The product was isolated with methanol under a nitrogen atmosphere. This compound is air and water stable, and is insoluble in common organic solvents. Semiquantitative microprobe analysis on a number of these crystals by SEM/EDS gave an average composition of $Rb_{1.0}Hg_{5.8}S_{7.5}$. A yield of 92%, based on HgS, is typical.

(i) $Cs_2Hg_6S_7$ (VI). Black needles of $Cs_2Hg_6S_7$ were obtained by the reaction of 2.161 g (7.3 mmol) of Cs_2S and 10.221 g (44 mmol) of HgS. This charge was sealed inside an evacuated quartz tube. The tube was placed inside a computer-controlled furnace and heated at 400 °C for 1.5 days, followed by heating at 500 °C for 1 day, slow cooling to 50 °C, and quenching to room temperature. The product was isolated with methanol under a nitrogen atmosphere. This compound is air and water stable, and is insoluble in common organic solvents. Semiquantitative microprobe analysis on a number of these crystals by SEM/EDS gave an average composition of $Cs_{1.5}Hg_{6.0}S_{7.6}$. A yield of 90%, based on HgS, is typical.

(j) $Rb_2Hg_6Se_7$ (VII). Black needles of $Rb_2Hg_6Se_7$ were obtained by the reaction of 0.816 g (3.3 mmol) of Rb_2Se and 5.5480 g (20 mmol) of HgSe. This charge was sealed inside an evacuated quartz tube. The tube was placed inside a computer-controlled furnace and heated at 550 °C for 2 days, followed by slow cooling to 150 °C and quenching to room temperature. The product was isolated with methanol under a nitrogen atmosphere. This compound is air and water stable, and is insoluble in common organic solvents. Semiquantitative microprobe analysis on a number of these crystals by SEM/EDS indicated the presence of Rb, Hg, and S. A yield of 85%, based on HgS, is typical.

(k) $Cs_2Hg_6Se_7$ (VIII). This compound could be prepared only by direct synthesis: 0.086 g (0.25 mmol) of Cs_2Se and 0.420 g (1.50 mmol) of HgSe were mixed together and loaded in a Pyrex tube that was then flame-sealed under vacuum ($\sim 10^{-3}$ mbar). The tube was placed in a computer-controlled furnace and heated at 375 °C for 72 h and cooled slowly to 50 °C at a rate of 3 °C/h. Black needle-shaped crystals were obtained. The product is not soluble in water and any common organic solvents. A quantitative microprobe analysis performed on a large number of crystals with the EDS/SEM system gave an average composition of $Cs_{2.1}Hg_{6.0}Se_{7.3}$.

(l) $Rb_2Hg_6S_{3.5}Se_{3.5}$ (IX). Black needles of $Rb_2Hg_6S_{3.5}Se_{3.5}$ were obtained by the reaction of 0.203 g (1.0 mmol) of Rb_2S, 0.249 g (1.0 mmol) of Rb_2Se, 1.396 g (6.0 mmol) of HgS, and 1.887 g (6.0 mmol) of HgSe. This charge was sealed inside an evacuated quartz tube. The tube was placed inside a computer-controlled furnace and heated at 650 °C for 2 days, followed by slow cooling to 50 °C and quenching to room temperature. The product was isolated with methanol under a nitrogen atmosphere. This compound is air and water stable, and is insoluble in common organic solvents. Semiquantitative microprobe analyses on a number of these crystals from different locations in the sample were consistent and verified the presence of Rb, Hg, Se, and S. A yield of 90%, based on HgSe and HgS, is typical.

(m) $Cs_2Hg_6S_{5.25}Se_{1.75}$ (X). Black needles of $Cs_2Hg_6S_{5.25}Se_{1.75}$ were obtained by the reaction of 0.222 g (0.75 mmol) of Cs_2S, 0.086 g (0.25 mmol) of Cs_2Se, 1.047 g (4.5 mmol) of HgS, and 0.472 g (1.5 mmol) of HgSe. This charge was sealed inside an evacuated fused silica tube. The tube was placed inside a computer-controlled furnace and heated at 650 °C for 2 days, followed by slow cooling to 50 °C and quenching to room temperature. The product was isolated with methanol under a nitrogen atmosphere. This compound is air and water stable, and is insoluble in common organic solvents. Semiquantitative microprobe analyses on a number of these crystals from different locations in the sample were consistent and verified the presence of Cs, Hg, Se, and S. A yield of 90%, based on HgSe and HgS, is typical. Other solid solutions were prepared similarly.

Crystallographic Studies. Single-Crystal X-ray Diffraction. The X-ray single-crystal data of $K_2Hg_3S_4$, $Cs_2Hg_3Se_4$, $K_2Hg_6S_7$, $Cs_2Hg_6S_7$, and $Cs_2Hg_6Se_7$ were collected on a Nicolet P3 four-circle diffractometer with graphite monochromated Mo−Kα radiation, using the $\theta-2\theta$ scan mode. The data for $K_2Hg_3Se_4$ were collected on an Enraf-Nonius CAD4 diffractometer with Mo Kα radiation, using the $\omega-2\theta$ scan mode by Dr. M. Sabat at Northwestern University. A Siemens SMART Platform CCD diffractometer was used to collect data from $Rb_2Hg_6S_7$ at 25 °C, using 80 s exposure time (crystal-detector distance 5 cm). An empirical absorption correction was applied to the data of $Rb_2Hg_6S_7$ (Blessing, R. H. *Acta Crystallogr*. **1995**, *A51*, 33−38). Accurate unit cell parameters for all compounds were obtained from the least-squares refinement of the angles of 20−25 machine-centered reflections with 2θ values between 10 and 30°. The stability of the experimental setup and crystal integrity were monitored by measuring three standard reflections periodically (every 100−150 reflections) during the data collection period. The data of $K_2Hg_3S_4$ showed appreciable decay (34.3% decay) due to decomposition of the crystal. The color of the crystal changed from yellow to gray during the data collection period. The other data sets did not show any appreciable decay. Two absorption corrections were applied to all data: an empirical absorption correction based on ψ scans for three reflections (with $\chi \sim 90°$) followed by a DIFABS correction according to the recommended protocol.[14] The structures of $K_2Hg_3S_4$, $K_2Hg_3Se_4$, $Cs_2Hg_3Se_4$, $K_2Hg_6S_7$, and $Cs_2Hg_6Se_7$ were solved with the direct methods of the SHELXS-86[15] software package and were refined with the SDP[16] package of crystallographic programs on a VAX station 2000 computer. The structures of $Rb_2Hg_6S_7$ and $Cs_2Hg_6S_7$ were solved with the direct methods of the SHELXS-86[15] software package and were refined with the TEXSAN[17] package of crystallographic programs on a VAX station 3100/76 computer. The effect of secondary extinction was considered in the least-squares refinement as an additional parameter due to the heavy atomic constituents of the crystals. All atoms except the sulfur atoms in $K_2Hg_3S_4$ and $Cs_2Hg_6S_7$ were refined anisotropically. The sulfur atoms in these two structures become nonpositive definite when refined anisotropically, and this is attributed to the crystal decay for $K_2Hg_3S_4$ and to the larger than average size for $Cs_2Hg_6S_7$ which resulted in insufficient correction for absorption. For $K_2Hg_6S_7$, $Rb_2Hg_6S_7$, $Cs_2Hg_7S_7$, and $Cs_2Hg_6Se_7$, the correct enantiomorph was assigned by determining which one resulted in the best refinement. Long exposure (1−2 h) axial photographs for all crystals showed no evidence of superstructure. The complete data collection parameters and details of the structure solution and refinement for all compounds are given in Tables 1−3. The final atomic coordinates, temperature factors, and their estimated standard deviations are given in Tables 4−10.

The compounds were examined by X-ray powder diffraction to check for phase purity and for identification. Powder patterns obtained on a Philips XRG-3000 powder diffractometer and a Rigaku rotating anode (Cu Kα) X-ray powder diffractometer, Rigaku-Denki/Rw400F2 (RotaFlex), provided accurate d_{hkl} spacings and showed that the set $K_2Hg_3S_4$, $K_2Hg_3Se_4$, and $Cs_2Hg_3Se_4$ and the set $Rb_2Hg_6S_7$, $Cs_2Hg_6S_7$, $Rb_2Hg_6Se_7$, and $Cs_2Hg_6Se_7$ are X-ray isomorphous. The calculated[18] and observed powder patterns of $K_2Hg_3S_4$, $K_2Hg_6S_7$, and $Cs_2Hg_6Se_7$ are given in Tables 11−13, respectively, while the rest have been deposited as Supporting Information.

Physical Measurements. (a) Semiquantitative Microprobe Analysis. Semiquantitative microprobe analyses was performed on a JEOL JSM-35C scanning electron microscope (SEM) equipped with a Noran Energy Dispersive Spectroscopy (EDS) system. Data acquisition was performed with an accelerating voltage of 20 kV. Compositions are the average of several 30 s acquisitions.

(14) Walker, N.; Stuart, D. *Acta Crystallogr*. **1983**, *39A*, 158.
(15) Sheldrick, G. M. In *Crystallographic Computing, 3*; Ed. Sheldrick, G. M., Kruger, C., Doddard, R., Eds.; Oxford University Press: Oxford, England, 1985; pp 175−189.
(16) Frenz, B. A. The Enraf-Nonius CAD4 SDP System. In *Computing in Crystallography*; Delft University Press: Delft, Holland, 1978; pp 64−71.
(17) TEXSAN: Single-Crystal Structure Analysis Software, Version 5.0; Molecular Structure Corp.: The Woodlands, TX 77381, 1981.
(18) Smith, D. K.; Nichols, M. C.; Zolensky, M. E. POWD10: A Fortran IV Program for Calculating X-ray Powder Diffraction Patterns, Version 10; Pennsylvania State University, 1983.

Table 1. Summary of Crystallographic Data for $K_2Hg_3S_4$, $K_2Hg_3Se_4$, and $Cs_2Hg_3Se_4$

formula	$K_2Hg_3S_4$	$K_2Hg_3Se_4$	$Cs_2Hg_3Se_4$
FW, g/mol	808.23	995.81	1183.42
color/habit	yellow/ hex. plate	red/hex. plate	orange/hex. plate
dimensions, (mm)	0.15 × 0.10 × 0.01	0.17 × 0.12 × 0.02	0.22 × 0.18 × 0.02
a, Å	10.561(5)	10.820(2)	12.047(4)
b, Å	6.534(3)	6.783(1)	6.465(2)
c, Å	13.706(2)	14.042(3)	14.771(6)
V, Å; *Z*	945.8(7); 4	1030.6(5); 4	1150.4(7); 4
space group	*Pbcn* (no. 60)	*Pbcn* (no. 60)	*Pbcn* (no. 60)
d_{calc}, g/cm^3	5.68	6.42	6.83
$\mu_{(MoK\alpha)}$, cm^{-1}	502.3	593.2	586.1
radiation	Mo Kα ($\lambda = 0.71069$ Å)	Mo Kα($\lambda = 0.71069$ Å)	Mo Kα($\lambda = 0.71069$ Å)
temp, °C	23	−120	23
scan type	$\theta/2\theta$	$\theta/2\theta$	$\theta/2\theta$
$2\theta_{max}$, deg	50	50	48
reflections:			
measd/unique	2829/831	1088/903	1058/900
no. of reflcns with $F_o^2 > 3\sigma(F_o^2)$	326	567	319
no. of variables	33	43	43
R/R_w[a]	5.7%/6.3%	7.7%/8.4%	5.5%/6.2%
extinction coeff	1.58×10^{-8}	2.06×10^{-8}	3.15×10^{-8}

[a] $R = \sum(|F_o| - |F_c|)/\sum|F_o|$. $R_w = \{\sum w(|F_o| - |F_c|)^2/\sum w|F_o|^2\}^{1/2}$. $w = 1/\sigma^2(F)$.

Table 2. Summary of Crystallographic Data for $K_2Hg_6S_7$ and $Rb_2Hg_6S_7$

formula	$K_2Hg_6S_7$	$Rb_2Hg_6S_7$
FW, g/mol	1506.19	1598.90
color/habit	black/needle	black/needle
dimensions, mm	0.04 × 0.04 × 0.46	0.26 × 0.01 × 0.01
a, Å	13.805(8)	13.9221(8) Å
b, Å	13.805(8)	13.9221(8) Å
c, Å	4.080(3)	4.1204(2) Å
V, Å; *Z*	778(1); 2	798.64(6); 2
space group	$P\bar{4}2_1m$ (no. 113)	$P\bar{4}_2nm$ (no. 102)
d_{calc}, g/cm^3	6.43	6.65
$\mu_{(MoK\alpha)}$, cm^{-1}	604.2	645.32
radiation	Mo Kα ($\lambda = 0.71069$ Å)	Mo Kα ($\lambda = 0.71069$ Å)
temp, °C	23	23
scan type	$\theta/2\theta$	
$2\theta_{max}$, deg	50	55
min/max abs coef for ψ scan corr	0.48/1.00	0.42/1.00
reflections:		
measured/unique	1614/453	2594/697
no. of reflcns with $F_o^2 > 3\sigma(F_o^2)$	402 (on 2σ)	441
no. of variables	42	41
R/R_w[a]	3.1%/3.6%	4.3%/4.0%
extinction coeff	1.50×10^{-7}	1.57×10^{-7}

[a] $R = \sum(|F_o| - |F_c|)/\sum|F_o|$. $R_w = \{\sum w(|F_o| - |F_c|)^2/\sum w|F_o|^2\}^{1/2}$. $w = 1/\sigma^2(F)$.

(b) Optical Spectroscopy. A Shimadzu UV-3101PC double beam, double-monochromator spectrophotometer was used to measure the room temperature, optical diffuse reflectance spectra of the five compounds. The methods used to collect the reflectance data and convert it to absorbance values have been described elsewhere.[19] We have obtained the bandgap values by extrapolating the linear regions of each $(a/S)^2$ versus energy plot to $(a/S)^2 = 0$.[20] These values are estimated to be accurate to ±0.03 eV.

(c) Differential Thermal Analysis. Thermal analysis was performed on a Shimadzu DTA-50 Differential Thermal Analyzer. High-quality crystals were selected from the reaction product and ground. Approximately 15 mg of each material was loaded into a 2.0 mm i.d. × 3.0 mm o.d. quartz tube with a flattened bottom and sealed under a vacuum of less than 1×10^{-4} mbar. Heating and cooling rates of 10 °C/min were used. Typically, the samples showed an endothermic peak upon heating and an exothermic peak upon cooling. The temperature associated with each thermal event was assigned to the melting and recrystallization, respectively, of each compound. Comparisons between powder patterns taken before and after heating were made to establish whether each compound melted with or without decomposition.

Results and Discussion

Dimensional Reduction of the Covalent HgQ Framework. The incorporation of A_2Q into the binary HgQ amounts to the introduction of Q^{2-} atoms in the diamond lattice of HgQ and the generation of anionic $[Hg_xQ_y]^{n-}$ frameworks. In essence the dense packed lattice of the binary compound is "diluted" with Q^{2-} atoms which progressively dismantle it. The A^+ acts as a noninterfering counterion. The chemical homology created in this way is of the type $(A_2Q)_m(HgQ)_n$ with the two end members being HgQ ($m = 0$, $n = 1$) and A_6HgQ_4 ($m = 3$, $n = 1$). The latter contains discrete tetrahedral $[HgQ_4]^{6-}$ anions and represents the maximum possible A_2Q equivalents around a Hg atom. As the Q^{2-}/Hg^{2+} ratio increases the dismantling of the original structure increases as well. This also leads to an attendant reduction in the coordination number of the chalcogen, which of course results in the dimensional reduction of the

(19) McCarthy, T. J.; Ngeyi, S−P.; Liao, J−H.; DeGroot, D. C.; Schindler, J.; Kannewurf, C. R.; Kanatzidis, M. G. *Chem. Mater.* **1993**, *5*, 331−340.

(20) Pankove, J. I. In Optical Processes in Semiconductors; Dover Publications: New York, 1975.

Table 3. Summary of Crystallographic Data for $Cs_2Hg_6S_7$ and $Cs_2Hg_6Se_7$

formula	$Cs_2Hg_6S_7$	$Cs_2Hg_6Se_7$
FW, g/mol	1693.77	2022.07
color/habit	black/needle	black/needle
dimensions (mm)	0.05 × 0.05 × 0.8	0.02 × 0.04 × 0.76
a, Å	13.958(4)	14.505(7)
b, Å	13.958(4)	14.505(7)
c, Å	4.159(2)	4.308(2)
V, Å; *Z*	810.2(8); 2	906(1); 2
space group	$P4_2nm$ (no. 102)	$P4_2nm$ (no. 102)
d_{calc}, g/cm^3	6.94	7.41
$\mu_{(MoK\alpha)}$, cm^{-1}	604.2	684.7
radiation	Mo Kα ($\lambda = 0.71069$ Å)	Mo Kα ($\lambda = 0.71069$ Å)
temp, °C	−80	23
scan type	$\omega/2\theta$	$\omega/2\theta$
$2\theta_{max}$, deg	60	44
min/max abs coef for ψ scan corr	0.78/1.00	0.536/1.00
reflections:		
measured/unique	2962/753	1440/604
reflections with $F_o^2 > 3\sigma(F_o^2)$	1752	530
no. of variables	49	41
R/R_w[a]	4.3%/4.4%	3.6/4.0
extinction coeff	5.31×10^{-8}	1.11×10^{-7}

[a] $R = \sum(|F_o| - |F_c|)/\sum|F_o|$. $R_w = \{\sum w(|F_o| - |F_c|)^2/\sum w|F_o|^2\}^{1/2}$. $w = 1/\sigma^2(F)$.

Table 4. Fractional Atomic Coordinates and B_{eq} Values for $K_2Hg_3S_4$ with Their Estimated Standard Deviations in Parentheses

atom	*x*	*y*	*z*	B_{eq},[a] Å^2
Hg(1)	0.34148(9)	0.0852(3)	0.2582(1)	1.48(3)
Hg(2)	0	0.0837(5)	1/4	1.77(5)
K	0.3788(6)	0.766(3)	0.5018(8)	1.8(2)
S(1)	0.3674(7)	0.175(2)	0.6416(8)	0.8(2)*
S(2)	0.3710(7)	0.362(2)	0.3678(8)	1.1(2)*

[a] *B* values for anisotropically refined atoms are given in the form of the isotropic equivalent displacement parameter defined as $B_{eq} = (4/3)[a^2B_{11} + b^2B_{22} + c^2B_{33} + ab(\cos\gamma)B_{12} + ac(\cos\beta)B_{13} + bc(\cos\alpha)B_{23}]$. Starred atoms were refined isotropically.

Table 5. Fractional Atomic Coordinates and B_{eq} Values for $K_2Hg_3Se_4$ with Their Estimated Standard Deviations in Parentheses

atom	*x*	*y*	*z*	B_{eq},[a] Å^2
Hg(1)	0.3383(2)	0.0889(3)	0 .2586(2)	2.74(4)
Hg(2)	0	0.0874(6)	1/4	2.77(6)
Se(1)	0.1338(5)	0.3239(9)	0 .1382(4)	2.2(1)
Se(2)	0.3723(6)	0.3649(8)	0 .3707(4)	2.3(1)
K	0.118(1)	0.270(2)	0 .501(1)	2.6(2)

[a] *B* values for anisotropically refined atoms are given in the form of the isotropic equivalent displacement parameter defined as $B_{eq} = (4/3)[a^2B_{11} + b^2B_{22} + c^2B_{33} + ab(\cos\gamma)B_{12} + ac(\cos\beta)B_{13} + bc(\cos\alpha)B_{23}]$.

Table 6. Fractional Atomic Coordinates and B_{eq} Values for $Cs_2Hg_3Se_4$ with Their Estimated Standard Deviations in Parentheses

atom	*x*	*y*	*z*	B_{eq},[a] Å^2
Hg(1)	0.3309(2)	0.0051(6)	0.2416(3)	3.66(4)
Hg(2)	0	−0.0123(9)	1/4	3.40(6)
Cs	0.1203(3)	0.2656(4)	0.5105(3)	2.94(6)
Se(1)	0.1234(5)	0.2316(7)	0.1353(4)	2.5(1)
Se(2)	0.3604(4)	0.2918(7)	0.3541(5)	2.2(1)

[a] *B* values for anisotropically refined atoms are given in the form of the isotropic equivalent displacement parameter defined as $B_{eq} = (4/3)[a^2B_{11} + b^2B_{22} + c^2B_{33} + ab(\cos\gamma)B_{12} + ac(\cos\beta)B_{13} + bc(\cos\alpha)B_{23}]$.

Table 7. Fractional Atomic Coordinates and B_{eq}[a] Values for $K_2Hg_6S_7$ with Estimated Standard Deviations in Parentheses

atom	*x*	*y*	*z*	B_{eq}
Hg1	0.56782(6)	0.34115(7)	0.7608(4)	2.65(2)
Hg2	0.90144(6)	0.59856	0.7238(4)	2.41(2)
K1	0.6713(4)	0.8287	0.764(3)	3.5(1)
S1	0.6965(4)	0.4650(4)	0.743(2)	1.8(1)
S2	0.0	0.5	0.061(4)	2.8(2)
S3	0.8139(4)	0.6861	0.330(2)	2.0(1)

[a] *B* values for anisotropically refined atoms are given in the form of the isotropic equivalent displacement parameters defined as $B_{eq} = (4/3)[a^2B_{11} + b^2B_{22} + c^2B_{33} + ab(\cos\gamma)B_{12} + ac(\cos\beta)B_{13} + bc(\cos\alpha)B_{23}]$.

Table 8. Fractional Atomic Coordinates and B_{eq}[a] Values for $Rb_2Hg_6S_7$ with Estimated Standard Deviations in Parentheses

atom	*x*	*y*	*z*	B_{eq}
Hg1	0.92937(3)	0.65555(3)	0.7894(4)	2.35(1)
Hg2	0.90098(3)	0.90098	1.2597(7)	4.16(1)
Rb1	0.67018(8)	0.67018	1.296(1)	2.57(2)
S1	1.0283(2)	0.6947(2)	1.310(7)	1.65(4)
S2	0.5	0.5	1.044(2)	2.83(9)
S3	0.8151(2)	0.8151	0.8189	2.11(4)

[a] *B* values for anisotropically refined atoms are given in the form of the isotropic equivalent displacement parameters defined as $B_{eq} = (4/3)[a^2B(1,1) + b^2B(2,2) + c^2B(3,3) + ab(\cos\gamma)B(1,2) + ac(\cos\beta)B(1,3) + bc(\cos\alpha)B(2,3)]$.

structure. If many members of the $(A_2Q)_m(HgQ)_n$ homology are known one can observe the successive dimensional changes in the system from dense three-dimensional motif to "porous" three-dimensional, to lamellar, and finally to discrete chains, clusters, and mononuclear complexes. Unfortunately there is no single family of compounds in which all members are known, but a glance can be obtained from the partial collections which are available, see for example the $Cat/Re_6S_8/X$,[8] $(A_2Q)_m(CdQ)_n$,[6] and $(A_2Q)_m(Bi_2Q_3)_n$[19,21] systems. The decreasing dimensionality with increasing *m* leads to an increasingly inhibited ability to extend orbital overlap in various directions in the lattice of the $[Hg_xQ_y]^{n-}$ frameworks which leads to narrowing of the bands and widening of the bandgaps. Therefore one may obtain materials in which quantum confinement may be present in certain crystallographic directions.[22] A simple diagram that illustrates the structural evolution from bulk HgQ to $[HgQ_4]^{6-}$

(21) (a) McCarthy, T. J.; Tanzer, T. A.; Kanatzidis, M. G. *J. Am. Chem. Soc.* **1995**, *117*, 1294−1301. (b) Kanatzidis, M. G.; McCarthy, T. J.; Tanzer, T. A.; Chen, L.-H.; Iordanidis, L.; Hogan, T.; Kannewurf, C. R.; Uher, C.; Chen, B. *Chem. Mater.* **1996**, *8*, 1465−1474.

Table 9. Fractional Atomic Coordinates and B_{eq}[a] Values for $Cs_2Hg_6S_7$ with Estimated Standard Deviations in Parentheses

atom	*x*	*y*	*z*	B_{eq}
Hg1	0.0739(1)	0.3474(1)	0.0580	1.10(7)
Hg2	0.0993(1)	0.0993	0.4640(9)	0.88(5)
Cs1	0.3311(2)	0.3311	−0.430(2)	1.07(8)
S1	0.1926(7)	0.4788(7)	0.071(4)	0.9(2)[b]
S2	0.5	0.5	−0.719(6)	0.5(3)[b]
S3	0.1821(7)	0.1821	0.066(6)	1.0(2)[b]

[a] *B* values for anisotropically refined atoms are given in the form of the isotropic equivalent displacement parameters defined as $B_{eq} = (4/3)[a^2B(1,1) + b^2B(2,2) + c^2B(3,3) + ab(\cos\gamma)B(1,2) + ac(\cos\beta)B(1,3) + bc(\cos\alpha)B(2,3)]$. [b] Isotropic temperature factors.

Table 10. Fractional Atomic Coordinates and B_{eq}[a] Values for $Cs_2Hg_6Se_7$ with Estimated Standard Deviations in Parentheses

atom	*x*	*y*	*z*	B_{eq}
Hg1	0.07503(9)	0.3488(1)	0.058	2.71(2)
Hg2	0.10077(9)	0.10077	0.4687(5)	2.42(2)
Cs1	−0.1686(2)	0.1686	0.063(1)	2.68(4)
Se1	0.0200(7)	0.6935(2)	0.556(1)	1.68(6)
Se2	0.5	0.5	0.285(2)	2.28(9)
Se3	0.3168(2)	0.6832	0.548(1)	1.66(5)

[a] *B* values for anisotropically refined atoms are given in the form of the isotropic equivalent displacement parameters defined as $B_{eq} = (4/3)[a^2B(1,1) + b^2B(2,2) + c^2B(3,3) + ab(\cos\gamma)B(1,2) + ac(\cos\beta)B(1,3) + bc(\cos\alpha)B(2,3)]$.

Table 11. Calculated and Observed Powder Patterns of $K_2Hg_3S_4$

hkl	d_{calc} (Å)	d_{obs} (Å)	$I/I_{o,obs}$ (%)
002	6.85	6.90	33
004	3.42	3.43	100
021	3.17	3.18	6
310	3.09	3.10	7
213	3.05	3.06	5
311	3.02	3.03	4
022	2.94	2.95	3
312	2.82	2.82	13
023	2.65	2.67	10
313	2.56	2.57	4
024	2.364	2.366	3
314	2.298	2.301	13
006	2.284	2.285	30
025	2.099	2.104	8
315	2.053	2.057	5
026	1.872	1.875	2
316	1.839	1.843	13
331	1.835	1.838	12
333	1.716	1.717	40
008	1.713	1.717	22
041	1.622	1.627	3
042	1.589	1.585	2
604	1.566	1.569	2

molecules is shown in Figure 1. The colors and optical spectroscopic properties of $A_2Hg_3Q_4$ and $A_2Hg_6Q_7$ can be rationalized within this framework.

Structure Description of the $A_2Hg_3Q_4$ Compounds. $K_2Hg_3S_4$, $K_2Hg_3Se_4$, and $Cs_2Hg_3Se_4$ are isostructural. They possess centrosymmetric one-dimensional $[Hg_3Q_4]_n^{2n-}$ chains. Two views of the unit cell of $A_2Hg_3Q_4$ are shown in Figure 2. The $[Hg_3Q_4]_n^{2n-}$ chains run parallel to the crystallographic *b*-axis. The makeup of this chain can be regarded as a one-dimensional assembly of distorted tetrahedral $[HgQ_4]^{6-}$ building blocks connected by two-coordinate Hg^{2+} ions as shown in Figure 3. Alternatively, it can be viewed as a one-dimensional spiro-polymer of eight-membered Hg_4Q_4 rings. There are two crystallographically distinct Hg atoms in the asymmetric unit. The Hg1 atom has linear geometry, while the Hg2 atom, situated on a crystallographic 2-fold axis, has distorted tetrahedral geometry. The Q−Hg−Q angles around the linear Hg1 atoms are 165.3(3)°, 164.2(2),° and 158.8(2)° for $K_2Hg_3S_4$, $K_2Hg_3Se_4$, and $Cs_2Hg_3Se_4$, respectively. These angles are smaller than those about the Hg atoms in HgS, at 172°.[22] These smaller angles result from a small distortion toward trigonal coordination

Table 12. Calculated and Observed Powder Patterns for $K_2Hg_6S_7$

hkl	d_{calc} (Å)	d_{obs} (Å)	$I/I_{o,obs}$ (%)
200	6.90	6.95	8
201	6.17	6.24	43
301	4.36	4.40	17
400	3.45	3.47	45
211	3.40	3.43	55
410	3.34	3.37	100
330	3.25	3.27	43
221	3.13	3.14	88
420	3.08	3.10	13
301	3.05	3.06	14
321	2.79	2.80	22
430	2.76	2.77	68
510	2.70	2.72	18
520	2.56	2.57	36
421	2.461	2.470	16
440	2.440	2.448	12
441	2.094	2.099	16
531	2.047	2.048	24
002	2.040	2.044	18
611	1.983	1.988	47
550	1.952	1.957	15
640	1.914	1.919	16
613	1.837	1.841	14
711, 551	1.761	1.765	51
810	1.712	1.716	18
731	1.657	1.660	15
432	1.641	1.644	9
830	1.616	1.619	21
522	1.596	1.597	4

Table 13. Calculated and Observed Powder Patterns for $Cs_2Hg_6Se_7$

hkl	d_{calc} (Å)	d_{obs} (Å)	$I/I_{o,obs}$ (%)
210	6.48	6.48	10
400	3.62	3.66	21
211	3.58	3.61	16
410	3.51	3.54	43
330	3.41	3.44	44
221	3.29	3.32	100
311	3.14	3.16	12
321	2.94	2.96	29
430	2.90	2.92	27
520	2.69	2.71	10
421	2.59	2.60	11
440	2.56	2.58	15
530	2.487	2.50	8
501, 431	2.406	2.419	17
540	2.265	2.295	8
002	2.154	2.162	42
611	2.086	2.097	42
631	1.933	1.941	31
701	1.867	1.877	14
711, 551, 402	1.852	1.860	29
641, 332	1.823	1.843	21
810	1.799	1.808	24
731	1.742	1.749	8
432	1.729	1.736	11
830	1.697	1.705	13
522	1.682	1.690	8
532	1.628	1.635	11

(22) (a) Ozin, G. A. *Adv. Mater.* **1992**, *4*, 612−649. (b) Reed, M. A. *Sci. Am.* **1993**, 118−123. (c) Ozin, G. A. *Supramol. Chem.* **1995**, *6*, 125−134.

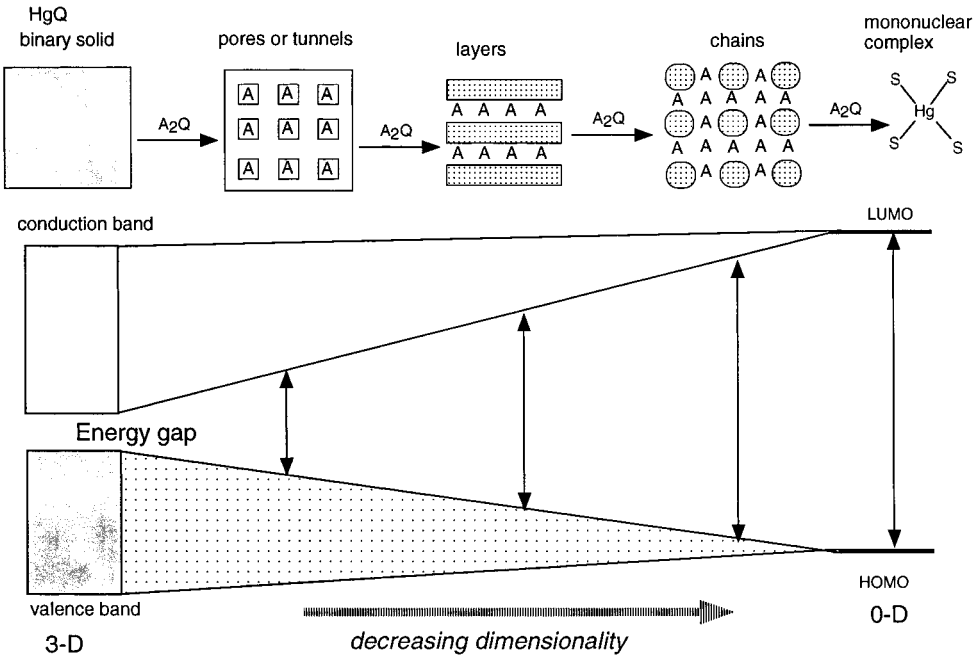

Figure 1. Schematic representation of progressive dimensional reduction in the structure of a dense binary semiconducting solid through "dilution" with A_2Q equivalents. The evolution of the energy bandgap is toward widening gaps with decreasing dimensionality.

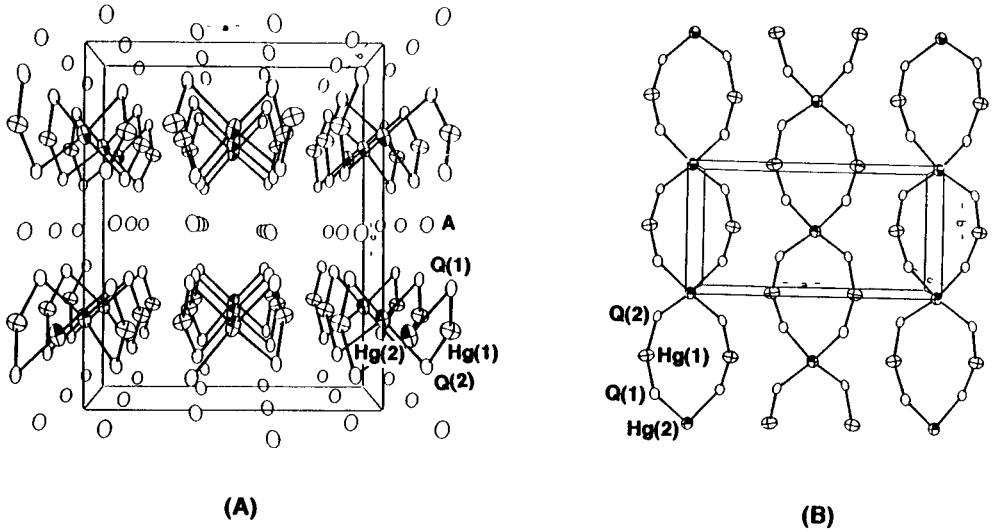

Figure 2. Two views of the unit cell of $A_2Hg_3Q_4$: (A) looking down the crystallographic *b* direction and (B) looking down the crystallographic *c* direction.

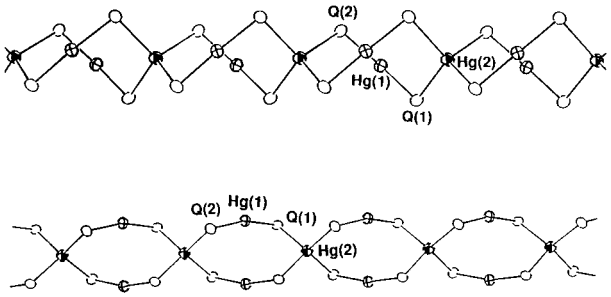

Figure 3. Two views of the one-dimensional $(Hg_3S_4)_n^{2n-}$ chains in $A_2Hg_3Q_4$.

geometry due to short Hg1−Q2 contacts between the chains. These contacts occur along the (001) plane, at distances of 3.08(1), 3.159(6), and 3.158(6) Å for $K_2Hg_3S_4$, $K_2Hg_3Se_4$, and $Cs_2Hg_3Se_4$, respectively. In this structure type, long Hg−Q bonds are associated with the tetrahedral Hg^{2+} centers, while shorter Hg−Q bonds are associated quasi-linear Hg^{2+} centers. The average Hg−Q bond distances for the tetrahedral Hg2 atoms are 2.57(1), 2.66(1), and 2.68(8) Å for $K_2Hg_3S_4$, $K_2Hg_3Se_4$, and $Cs_2Hg_3Se_4$, respectively. The value observed in $K_2Hg_3S_4$ is comparable to the distances of 2.542 and 2.592 Å reported for K_6HgS_4.[7] The Hg−S bonds for the quasilinear Hg1 atoms are 2.37(1), 2.48(1), and 2.47(6) Å for $K_2Hg_3S_4$, $K_2Hg_3Se_4$, and $Cs_2Hg_3Se_4$, respectively. The value observed in $K_2Hg_3S_4$ is slightly longer than the distances of 2.308(5) and 2.312(5) Å reported for K_2HgS_2.[9] Selected bond distances and angles for the three compounds are given in Tables 14and 15, respectively. There is one crystallographically distinct alkali metal in the asymmetric unit of each compound. The charge balancing alkali metal cations, A^+ ions (A = K, Cs), are distributed between the chains. They participate in ionic interactions with the chalcogenides.

It is interesting to comment on the structural difference between $Cs_2Hg_3Se_4$ and $Rb_2Hg_3Te_4$.[12] The latter compound was found to be layered but the structural makeup of the layers is

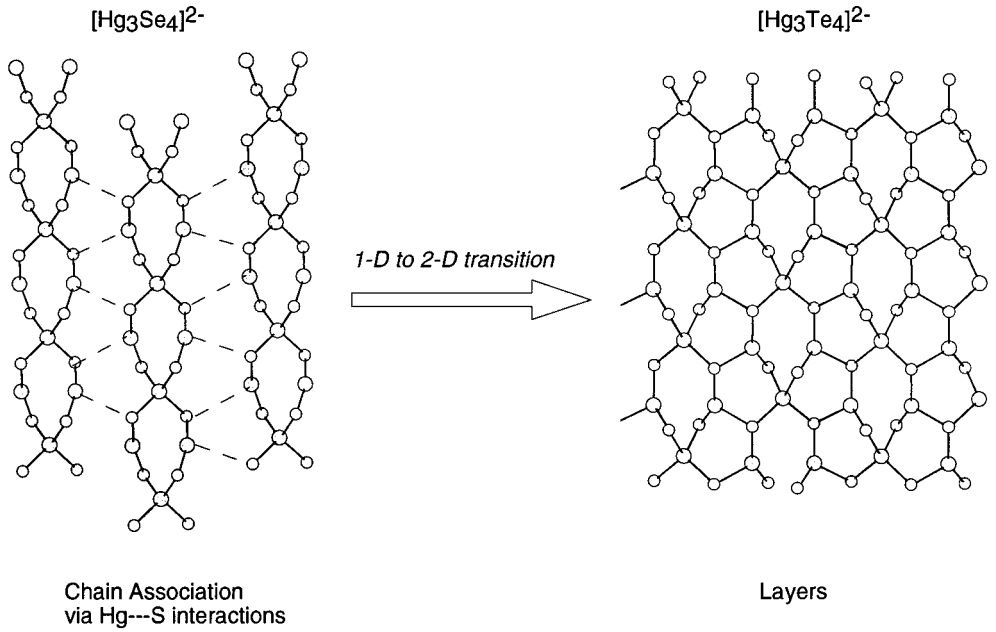

Figure 4. The transition from infinite $(Hg_3Se_4)_n^{2n-}$ chains to $(Hg_3Te_4)_n^{2n-}$ layers is straightforward through interchain Hg−Q interactions. This associative transformation converts the linearly coordinated Hg atoms to trigonal planar.

Table 14. Selected Bond Distances (Å) or $K_2Hg_3S_4$, $K_2Hg_3Se_4$, and $Cs_2Hg_3Se_4$ with Standard Deviations in Parentheses[a]

distance	$K_2Hg_3S_4$	$K_2Hg_3Se_4$	$Cs_2Hg_3Se_4$
Hg1−Q1	2.36(1)	2.486(6)	2.429(7)
Hg1−Q2	2.38(1)	2.473(6)	2.515(7)
Hg2−Q1	2.58(1)	2.671(6)	2.751(6)
Hg2−Q2	2.57(1)	2.657(6)	2.608(6)
Hg1−Q1	3.08(1)	3.159(6)	3.158(6)
Hg1−Q1	3.15(2)	3.210(6)	3.295(6)
A1−Q1	3.29(2)	3.37(1)	3.596(7)
A1−Q1	3.35(1)	3.37(1)	3.647(7)
A1−Q1	3.28(1)	3.37(1)	3.706(6)
A1−Q1	3.34(1)	3.38(1)	3.737(6)
A1−Q2	3.22(2)	3.30(2)	3.706(5)
A1−Q2	3.30(1)	3.36(1)	3.734(7)
A1−Q2	3.27(1)	3.35(1)	3.844(7)

Table 15. Selected Bond Angles (deg) for $K_2Hg_3S_4$, $K_2Hg_3Se_4$, and $Cs_2Hg_3Se_4$ with Standard Deviations in Parentheses[a]

angle	$K_2Hg_3S_4$	$K_2Hg_3Se_4$	$Cs_2Hg_3Se_4$
Q1−Hg1−Q2	165.3(3)	164.2(2)	158.8(2)
Q1−Hg2−Q1	104.7(3)	115.7(2)	110.1(2)
Q1−Hg2−Q2	105.7(3)	104.4(2)	105.3(2)
Q1−Hg2−Q2	114.9(9)	110.7(2)	107.0(2)
Q2−Hg2−Q2	111.0(4)	106.2(2)	121.9(3)
Hg1−Q1−Hg2	96.5(4)	95.7(2)	98.2(2)
Hg1−Q2−Hg2	95.8(4)	95.8(2)	93.5(2)

the result of associative bonding interactions of the parallel chains of $[Hg_3Q_4]_n^{2n-}$ in which Q atoms from one chain bind to linear Hg atoms of a neighboring chain, as illustrated in Figure 4. Given that the $[Hg_3Te_4]_n^{2n-}$ framework is larger in volume than the $[Hg_3Se_4]_n^{2n-}$, it is tempting to attribute the origin of this structural transition to the counterion effect. While a certain counterion may have the ability to screen properly anionic species of a given size and shape, a smaller set of counterions of equal charge may not be able to do so, thus causing the anionic species to associate. These associative interactions can lead to higher dimensionalities in the anionic part of the structure even though the stoichiometry of atoms in it remains constant. Conversely, the increase in size and volume of the anionic part of a structure without a concomitant increase in the volume of the countercation, can cause similar structural changes. The counterion effect also seems to explain the transition to a two-dimensional structure in going from $K_2Hg_3S_4$ to $Na_2Hg_3S_4$.[10]

The K^+ ions are surrounded by six chalcogen atoms in the range of 3.22(2)−3.35(1) and 3.30(2)−3.37(1) Å in $K_2Hg_3S_4$ and $K_2Hg_3Se_4$, respectively, while Cs^+ ions in $Cs_2Hg_3Se_4$ are surrounded by seven selenium atoms in the range of 3.596(7)−3.844(7) Å.

Structure Description of the $A_2Hg_6S_7$ Compounds. The $A_2Hg_6Q_7$ feature unique structure types with three-dimensional (3-D) frameworks and two kinds of parallel tunnels, see Figure 5. In fact the compounds adopt two different variants of what is essentially the same architectural motif. So $K_2Hg_6S_7$ crystallizes in the space group $P\bar{4}2_1m$ while $Rb_2Hg_6S_7$, $Cs_2Hg_6S_7$, and $Cs_2Hg_6Se_7$ belong to the space group $P4_2nm$. These two groups differ in the bonding of the corresponding Hg2 and S3 atoms. The K compound has linear and tetrahedral Hg^{2+} ions bridged by three crystallographically unique Q^{2-} ions, while the other three compounds have trigonal planar and tetrahedral Hg^{2+} centers also bridged by three crystallographically unique Q^{2-} ions. Every atom in the asymmetric unit has the same point symmetry in both space groups.

There are two kinds of easily recognizable one-dimensional tunnels running parallel to the crystallographic *c* axis. A set of empty, narrow tunnels with an octagonal cross section is composed of distorted tetrahedral Hg1 and trigonal pyramidal Q1 ions. The diameters of these tunnels are approximately 4.8−4.9 Å, corresponding to the Hg1−Hg1 distance. A second set of "stuffed", wider tunnels, of dimensions 6.14 × 5.26 Å, has a 12-member ring cross section in which both tetrahedral Hg1 and linear Hg2 atoms are held together by triply and doubly bridging Q^{2-} ions. The major difference between the two structures is the symmetry element passing through the center of the empty tunnels: a 4-fold inversion axis ($\bar{4}$) in $K_2Hg_6S_7$ versus a 4-fold screw axis (4_2) in the rest of the compounds. The two structures are related by an origin shift in the *a*-axis direction by $^1/_2$. The geometries of the doubly bridging Q2 and the triply bridging Q1 atoms are chevron-shaped and trigonal pyramidal, respectively. The other chalcogen atom Q3 differs in its binding between the K and the Rb compound.

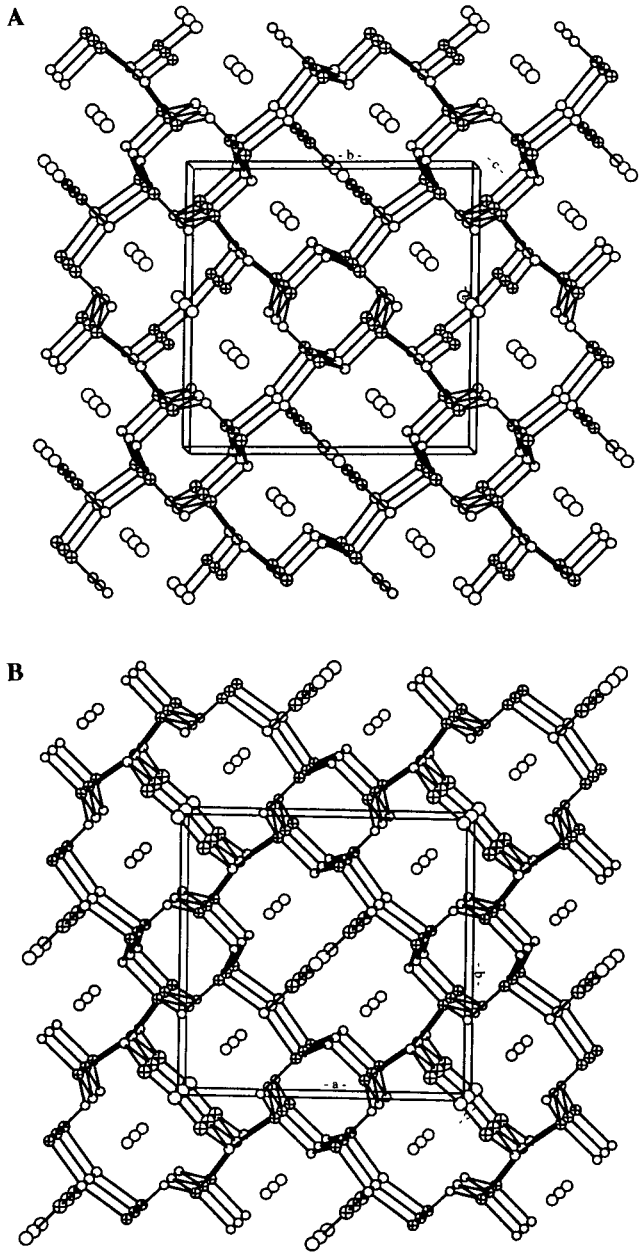

Figure 5. The unit cells of (A) $K_2Hg_6S_7$ and (B) $Rb_2Hg_6S_7$. Both views are down the crystallographic *c* direction. Hg, crossed ellipsoids; S, bonded, open ellipsoids; and K, isolated, open ellipsoids.

In $K_2Hg_6S_7$ the Q3 has a T-type coordination, while in $Rb_2Hg_6S_7$ the same atom has a "seesaw" geometry bonding to two Hg(2) and two Hg(1) atoms, see Figure 6. The seesaw geometry is obtained by displacing the Q3 atom in the structure of $K_2Hg_6S_7$ away from the plane defined by the atoms Hg(2)−Hg(1)−Hg(1). It is this displacement along the *c* axis that imposes lower symmetry on the frameworks of $Rb_2Hg_6S_7$, $Cs_2Hg_6S_7$, $Rb_2Hg_6Se_7$, and $Cs_2Hg_6Se_7$, by destroying the 2_1 screw-axis in the cell, causing a departure from the $P\bar{4}2_1m$ space group, see Figure 7. Notice that a mere destruction of the 2_1 screw-axis leads to the nonisomorphic space group $P\bar{4}$. The *n*-glide plane, required by the $P\bar{4}2_1nm$ space group, is obtained when the translation of the Q3 atom along the *z* axis reaches a point where all Q3 have the same *z* coordinate. At this point the Q3 atom still does not have equal Hg(2)−Q(3) distances in the structure, see Table 16. Both space groups $P4_2nm$ and $P\bar{4}2_1m$ are derivatives of the same minimal nonisomorphic super group $P4_2/mnm$.

The Hg1−S3−Hg1 and Hg1−S3−Hg2 angles in $K_2Hg_6S_7$ are 158.1(3)° and 100.9(2)°, respectively. The Hg1−Q3−Hg1 and Hg1−Q3−Hg2 angles in $Rb_2Hg_6S_7$, $Cs_2Hg_6S_7$, $Rb_2Hg_6Se_7$, and $Cs_2Hg_6Se_7$ are generally both smaller: for example, 156.2(1)° and 97.5(1)° respectively for $Cs_2Hg_6Se_7$. The Hg1−Q3 bonds are unusually long, varying from 2.718(4) to 2.879(2) Å in $K_2Hg_6S_7$ and $Cs_2Hg_6Se_7$, respectively, while the Hg2−Q3 bonds are normal (for a linear and trigonal planar coordinated Hg^{2+} ion), ranging from 2.345(8) to 2.477(5) Å for $K_2Hg_6S_7$ and $Cs_2Hg_6Se_7$, respectively. Selected bond distances and angles are given in Tables 16 and 17, respectively.

There is one crystallographically distinct alkali metal in each of the asymmetric units of the compounds. The alkali cations are found inserted in the center of the large 12-member tunnels, interacting with the chalcogenide lone pairs on electrons that are directed toward the tunnel center. The alkali ions are surrounded by seven chalcogen atoms in the range of 3.30(1) to 3.764(5) Å.

A view of $K_2Hg_6S_7$ and $Rb_2Hg_6S_7$ down their respective crystallographic [110] direction displays dramatically how all the Q2 atoms point in the same direction, see Figure 8. The acentric nature of these new compounds suggests the possibility that they may be useful as nonlinear optical materials, for second harmonic generation (SHG). Investigations are in progress to determine their properties in this regard.

Optical Spectroscopy. All of the $A_2Hg_6Q_7$ compounds possess larger bandgaps than their corresponding cubic HgQ parent compounds, see Figure 9. The absorption spectra of $K_2Hg_6S_7$, $Rb_2Hg_6S_7$, $Cs_2Hg_6S_7$, $Rb_2Hg_6Se_7$, $Cs_2Hg_6Se_7$, and their solid solutions display steep absorption edges that are the result of charge-transfer excitations between a Q p-like valence band and a Hg 6s-like conduction band, similar to those occurring in red HgS. The bandgaps have increased from 0 eV in cubic HgS[20] to 1.50, 1.55, and 1.61 eV in $K_2Hg_6S_7$,[23] $Rb_2Hg_6S_7$, and $Cs_2Hg_6S_7$, respectively, and from −0.15 eV in HgSe[20] to 1.13 and 1.17 eV in $Rb_2Hg_6Se_7$ and $Cs_2Hg_6Se_7$, respectively. To get sharp absorption spectra high purity HgS and HgSe must be used in the synthesis, otherwise "tailing" is observed below the bandgap arising from impurity mid-gap states.

The bandgaps mentioned above are consistent with the colors of the materials. The sulfides are dark red to black in color, while the selenides are black. This dramatic change from near zero gap in the HgQ to the intermediate gap semiconductor in the ternaries is attributed to the breakup of the parent structure. The result is more open 3-D framework with reduced covalent bonding because of lower coordination numbers in Hg and Q atoms in the structure and the fact that the high energy s and p orbitals of the alkali metal ions do not contribute to the band dispersion near the Fermi level. Band dispersion in these materials is, therefore, expected to be narrower than that in the binary HgQ compounds. This effect has been noted in $K_2Cd_2S_3$[5] the $A_2Cd_3Q_4$[6] compounds, and in the Cat^+/Pb/I system.[24]

The $A_2Hg_6Q_7$ compounds form solid solution compounds between the S and Se end members. Several members of these compounds were prepared and their lattice parameters were found to obey Vegard's law. In the solid solution compound $Rb_2Hg_6Se_{3.5}S_{3.5}$, a bandgap of 1.3 eV was observed. It is at a value halfway between those of the end members, $Rb_2Hg_6Se_7$ (1.13 eV) and $Rb_2Hg_6S_7$ (1.55 eV), and suggests that the $Rb_2Hg_6Se_{7-x}S_x$ system possesses a tunable bandgap. The $Cs_2Hg_6Se_{7-x}S_x$ system also demonstrates the same character-

(23) An extended Hückel band structure calculation on $K_2Hg_6S_7$ shows that bandgap in this material is direct. J. Li and M. G. Kanatzidis, unpublished work.

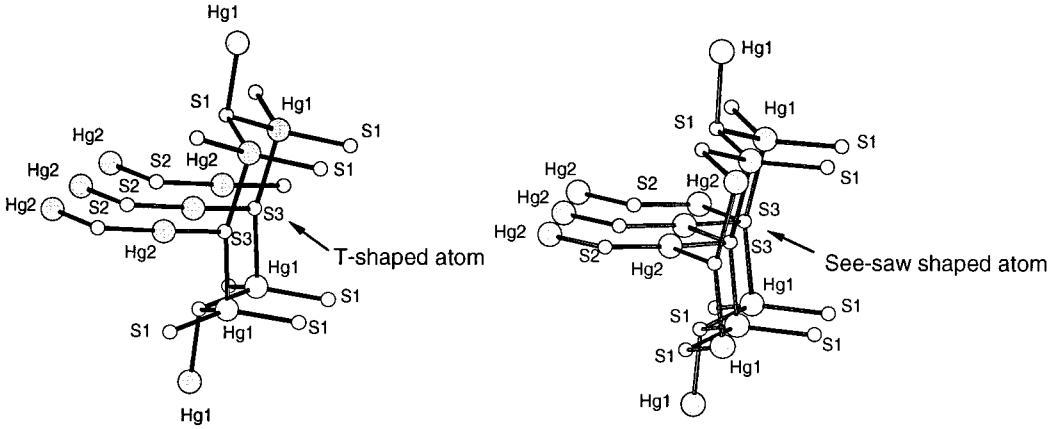

Figure 6. The T-type coordination of Q3 in the $A_2Hg_6Q_7$ compounds.

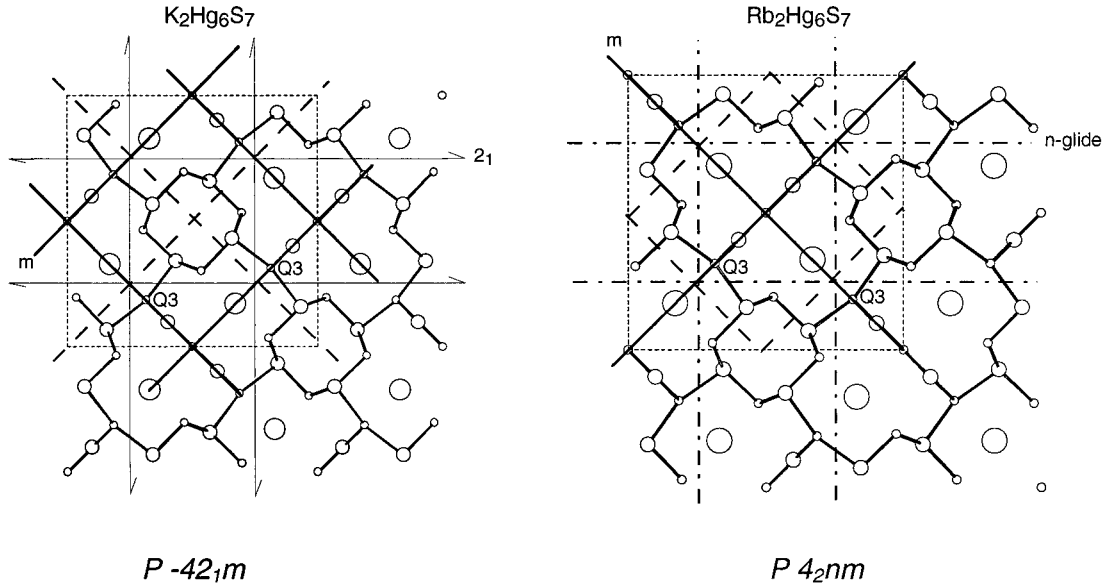

Figure 7. Space group comparison of the structurally similar but crystallographically different $K_2Hg_6S_7$ and $Rb_2Hg_6S_7$ looking down the *c* axis. The *n*-glide plane in $P4_2nm$ is generated by moving the Q3 atoms in the $P\bar{4}2_1m$ structure along the *z* axis so that they all attain the same *z* coordinate. At this point the $\bar{4}$ axis evolves into a 4_2 axis.

Table 16. Selected Bond Distances (Å) or $K_2Hg_6S_7$, $Rb_2Hg_6S_7$, $Cs_2Hg_6S_7$, and $Cs_2Hg_6Se_7$ with Standard Deviations in Parentheses[a]

distance	$K_2Hg_6S_7$	$Rb_2Hg_6S_7$	$Cs_2Hg_6S_7$	$Cs_2Hg_6Se_7$
Hg1−Q1	2.467(5)	2.518(9)	2.472(9)	2.637(4)
Hg1−Q1	2.552(8)	2.564(1)	2.574(7)	2.622(4)
Hg1−Q1	2.527(8)	2.475(4)	2.485(8)	2.564(3)
Hg1−Q3	2.718(4)	2.7322(6)	2.757(7)	2.870(2)
Hg1−Q3	2.718(5)	2.7322(6)	2.757(7)	2.870(2)
Hg2−Q2	2.366(9)	2.275(7)	2.362(9)	2.476(4)
Hg2−Q3	2.345(8)	2.57(1)	2.327(9)	2.477(5)
Hg2−Q3	3.007(9)	2.76(1)	2.988(9)	2.477(5)
A1−Q1	3.34(2)	3.450(8)	3.51(1)	3.664(4)
A1−Q1	3.30(1)	3.450(8)	3.51(1)	3.626(4)
A1−Q2	3.420(6)	3.508(5)	3.544(9)	3.660(3)
A1−Q3	3.30(1)	3.50(1)	3.59(2)	3.764(5)
A1−Q3	3.62(1)	3.54(1)	3.59(2)	3.690(5)

istics. A sample with the composition $Cs_2Hg_6Se_{1.75}S_{5.25}$ possesses a bandgap of 1.4 eV. The absorption spectra of some of these solid solutions are displayed in Figure 9. In fact, all the members examined in the $Rb_2Hg_6S_{7-x}Se_x$ series obey Vegard's law. These characteristics make these systems interesting for examination in cascade solar cells, waveguides, and other optoelectronic devices. Solid solutions of the type $Cs_2Hg_6Te_{7-x}Se_x$ should also be possible, although at some *x* value, the $Cs_2Hg_6Se_7$ structure is expected to become unstable, since we have been unsuccessful in isolating "$Cs_2Hg_6Te_7$".[25]

The $A_2Hg_3Q_4$ compounds are also semiconductors. Their great air sensitivity has inhibited an accurate determination of their bandgaps. The yellow color of $K_2Hg_3S_4$ suggests a bandgap of 2.5−2.6 eV, while the red and orange colors of $K_2Hg_3Se_4$ and $Cs_2Hg_3Se_4$ suggest bandgaps of about 2.1 and 2.2−2.3 eV, respectively. These materials definitely possess higher bandgaps than the $A_2Hg_6Q_7$ compounds which can be rational-

(24) (a) Ishihara, T.; Takahashi, J.; Goto, T. *Phys. Rev. B* **1990**, *42*, 11099−11107. (b) Papavassiliou, G. C.; Patsis, A. P.; Lagouvardos, D. J.; Koutselas, L. B. *Synth. Met.* **1993**, *55*−*57*, 3889−3894. (c) Hong, X.; Ishihara, T.; Nurmikko, A. V. *Phys. Rev. B* **1992**, *45*, 6961−6964. (d) Ishihara, T.; Takahashi, J.; Goto, T. *Solid State Commun.* **1989**, *69*, 933−936. (e) Papavassiliou, G. C.; Koutselas, J. B.; Lagouvardos, D. J. *Z. Naturforsch.* **1993**, *48b*, 1013−1014. (f) Vincent, B. R.; Robertson, K. N.; Camaron, T. S.; Knop, O. *Can. J. Chem.* **1987**, *65*, 1042−1046. (g) Nagapetyan, S. S.; Dolzhenko, Yu. I.; Arakelova, E. R.; Koshkin, V. M.; Struchkov, Yu. T.; Shklover, V. E. *Russ. J. Inorg. Chem.* **1988**, *33*, 1614−1618. (h) Poglitsch, A.; Weber, D. *J. Chem. Phys.* **1987**, *87*, 6373−6378. (i) Xu, C-Q.; Sakakura, H.; Kondo, T.; Takeyama, S.; Miura, N.; Takahashi, Y.; Kumata, K.; Ito, R. *Solid State Commun.* **1991**, *79*, 249−253. (j) Xu, C-Q.; Kondo, T.; Sakakura, H.; Kumata, K.; Takahashi, Y.; Ito, R. *Solid State Commun.* **1991**, *79*, 245−248. (k) Era, M.; Morimoto, S.; Tsutsui, T.; Saito, S. *Synth. Met.* **1995**, *71*, 2013−2014.

(25) Instead we have obtained $Cs_2Hg_3Te_4$, which has a different structure from that of $Cs_2Hg_3Se_4$ and is more closely related to that of $K_2Zn_3S_4$. See refs 6 and 7.

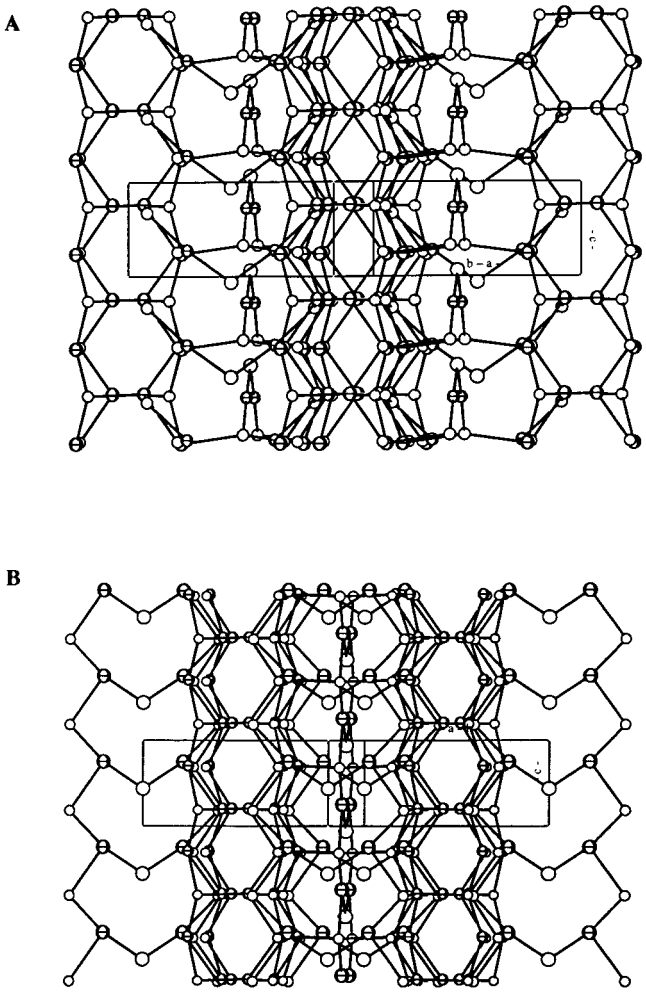

Figure 8. The $(Hg_6Q_7)_n^{2n-}$ frameworks of (A) $K_2Hg_6Q_7$ and (B) $Rb_2Hg_6S_7$. Both views are down the respective crystallographic [1, 1, 0] directions.

Table 17. Selected Bond Angles (deg) for $K_2Hg_6S_7$, $Rb_2Hg_6S_7$, $Cs_2Hg_6S_7$, and $Cs_2Hg_6Se_7$ with Standard Deviations in Parentheses[a]

angle	$K_2Hg_6S_7$	$Rb_2Hg_6S_7$	$Cs_2Hg_6S_7$	$Cs_2Hg_6Se_7$
Q1−Hg1−Q1	121.2(2)	121.4(4)	119.2(1)	121.3(1)
Q1−Hg1−Q1	124.8(3)	123.0(4)	122.8(6)	121.9(1)
Q1−Hg1−Q1	106.9(2)	108.6(1)	110.6(6)	110.0(1)
Q1−Hg1−Q3	96.3(2)	100.11(9)	96.5(1)	94.5(1)
Q1−Hg1−Q3	93.7(2)	98.1(3)	95.3(6)	95.9(1)
Q1−Hg1−Q3	106.5(2)	100.11(9)	104.7(7)	104.8(1)
Q2−Hg2−Q3	172.4(4)	162.2(4)	168.5(6)	166.4(2)
Hg1−Q1−Hg1	105.2(2)	108.6(1)	105.3(7)	110.0(1)
Hg1−Q1−Hg1	106.9(2)	108.6(1)	110.6(8)	103.7(1)
Hg1−Q1−Hg1	102.6(3)	103.2(3)	102.7(5)	103.2(1)
Hg2−Q2−Hg2	108.8(6)	117.9(5)	112.2(9)	113.2(3)
Hg1−Q3−Hg1	158.1(3)	161.22(3)	156.4(8)	156.2(1)
Hg1−Q3−Hg2	100.9(2)	96.2(3)	98.7(8)	97.5(1)
Hg2−Q3−Hg2	108.8(6)	101.13(5)	102.5(8)	102.8(1)

ized on the basis of both bulk dimensionality and framework connectivity at the atomic level. The $A_2Hg_6Q_7$ compounds possess tunneled, 3-D structures, while the $A_2Hg_3Q_4$ compounds have linear chain anions. The more interrupted the covalent bonding in HgQ becomes, the larger the bandgap is expected to be.[6] The higher bandgaps in the $A_2Hg_3Q_4$ compounds can also be rationalized by considering the coordination numbers of the mercury atoms in the two structural classes. In the $A_2Hg_3Q_4$ compounds, there are two linear mercury atoms for every one tetrahedral mercury atom, while these numbers are reversed in the $A_2Hg_6Q_7$ family. All of the Q atoms in the former family

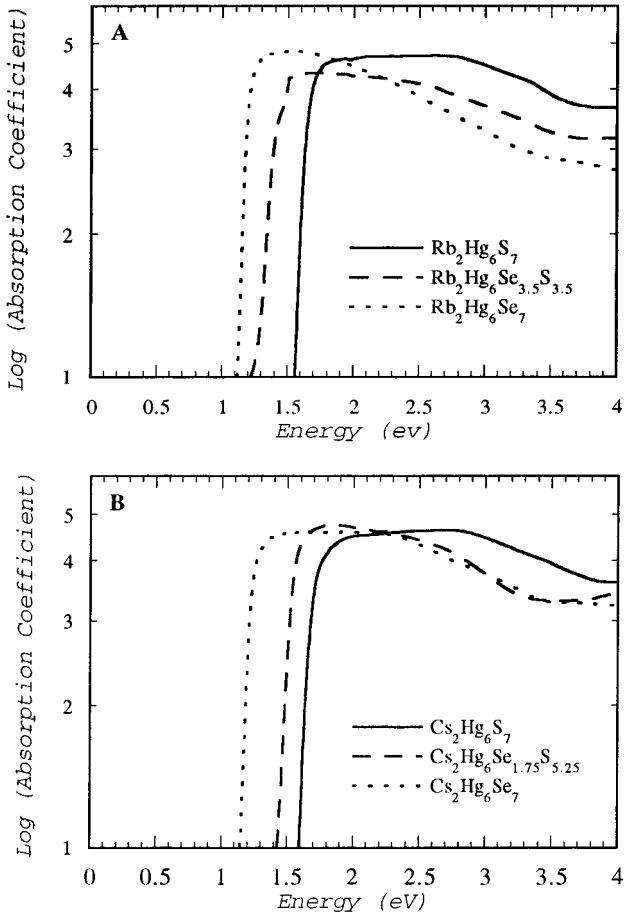

Figure 9. Solid-state absorption spectra of (A) $Rb_2Hg_6Se_7$, $Rb_2Hg_6Se_{3.5}S_{3.5}$, and $Rb_2Hg_6S_7$ and (B) $Cs_2Hg_6Se_7$, $Cs_2Hg_6Se_{1.75}S_{5.25}$, and $Cs_2Hg_6S_7$.

are in two-coordinate, chevron-shaped coordination, while in the latter, only $^1/_7$ of the Q atoms are two coordinate, with others in trigonal pyramidal or T-shaped geometries, as described above. Therefore, the generally lower connectivity of the $A_2Hg_3Q_4$ compounds at the atomic level can also be seen to result in the higher bandgaps. This trend is expected to continue, with the A_6HgQ_4 and the A_2HgQ_2 compounds possessing higher bandgaps than the $A_2Hg_3Q_4$ compounds. The former two structure types contain isolated HgQ_4^{6-} tetrahedra and isolated, linear HgQ_2^{2-} "dumbbell" anions, respectively.

Thermal Properties. Differential thermal analysis (DTA) was used to evaluate the thermal properties of these materials. Upon heating, $K_2Hg_6S_7$, $Rb_2Hg_6S_7$, $Cs_2Hg_6S_7$, $Rb_2Hg_6Se_7$, and $Cs_2Hg_6Se_7$ showed endothermic peaks centered at 556, 587, 586, 554, and 567 °C, respectively. These peaks correspond to melting transitions and are followed by exothermic crystallization peaks upon cooling at 472, 562, 542, 528, and 547 °C, respectively. In Figure 10, a representative DTA thermogram for $Cs_2Hg_6S_7$ is displayed, with the temperature and interpretation of each peak included. After the analysis, the presence of a tiny polycrystalline ingot instead of a loose powder provided assurance that the material had indeed melted. X-ray powder patterns were used for compound identification. All compounds but $Rb_2Hg_6Se_7$ melted congruently. The X-ray powder pattern of this compound becomes much simpler after the DTA experiment, suggesting degradation to HgSe.

The thermal properties of these new mercury chalcogenides appear to depend on the amount of sample and container size. The small amount of sample and the tube in the DTA experiment does not yield detectable byproducts after melting and recrys-

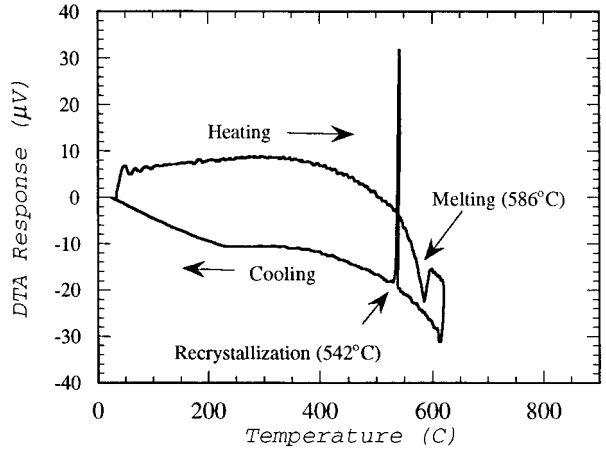

Figure 10. Differential thermogram of $Cs_2Hg_6S_7$. Heating/cooling rate of 10 °C/min.

tallization. Scale-up to bulk size samples, however, has been inhibited by the formation of HgQ or elemental Hg itself at temperatures 50−100 °C above the melting points of the materials. Preliminary attempts to grow large single crystals of $Cs_2Hg_6S_7$ in a vertical Bridgman type furnace resulted in directional solidification, which formed a dense agglomeration of parallel thin needles with their long axis (*c* axis) parallel to the growth direction.

Ion-Exchange Properties of $A_2Hg_6Q_7$. The alkali ion-filled infinite tunnels in the 3-D structure of $A_2Hg_6Q_7$ prompted us to ask whether they would be amenable to ion-exchange chemistry. This was particularly interesting to us because the lithium compound $Li_2Hg_6S_7$ could not be prepared under our synthetic flux conditions. At first, attempts were made using the rubidium sulfide analogue with aqueous and nonaqueous solutions of Li salts to obtain $Li_2Hg_6S_7$. These reactions were unsuccessful mainly because the large hydration (or solvation) sphere of Li renders it too large for the tunnel and kinetically inert. Recently, we reported a new convenient, low-temperature method, which serves to exchange, topotactically, large alkali ions for smaller ones by using alkali iodide salts.[26] This method involves the solid-state reaction at $T < 120$ °C of the host material with great excess LiI for several days, according to eq 1.

$$Rb_2Hg_6S_7 + LiI \rightarrow Li_2Hg_6S_7 + RbI \qquad (1)$$

The exceptional advantage of this reaction is (a) the low temperature, which prevents the destruction of the host material (should the material be unstable at higher temperatures), and (b) the absence of solvent, which avoids cation solvation. With this reaction 90% Rb exchange can be achieved, giving rise to $Li_{1.8}Rb_{0.2}Hg_6S_7$. Figure 11 shows a comparison of the X-ray powder diffraction patterns of parent and the ion-exchanged material and suggests a topotactic ion-exchange. Given that the tunnels in $Rb_2Hg_6S_7$ are relatively small and completely filled, and are only accessible by their two open ends (front and back of tunnel) and not via side openings, that ion-exchange happens at all is quite remarkable. The new compound $Li_{1.8}Rb_{0.2}Hg_6S_7$ has a dramatically decreased optical bandgap of 0.78 eV with respect to the 1.55 eV of $Rb_2Hg_6S_7$, see Figure 12. This decrease is attributed to considerably greater covalent bonding interactions of the Li ion with the sulfur atoms of the framework, in sharp contrast with the heavier alkali analogues in which the same interactions are primarily ionic. Similar effects are observed for the Se analogues. Further characterization of the ion-exchanged material is in progress.

(26) Chondroudis, K.; Kanatzidis, M. G. Submitted for publication.

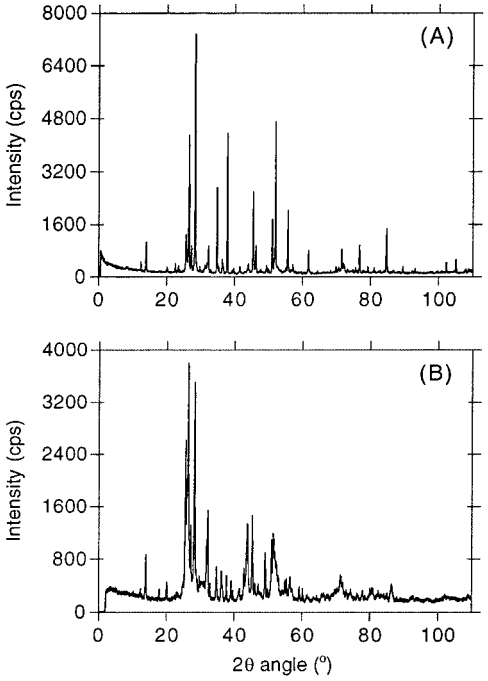

Figure 11. Comparison of the X-ray powder diffraction patterns of $Rb_2Hg_6S_7$ and $Li_{1.8}Rb_{0.2}Hg_6S_7$.

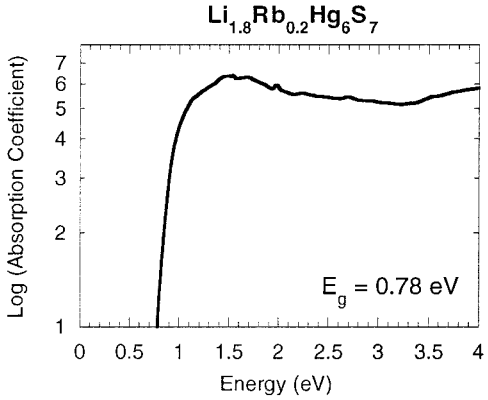

Figure 12. The optical absorption spectrum of $Li_{1.8}Rb_{0.2}Hg_6S_7$.

Concluding Remarks

The introduction of A_2Q into HgQ breaks up its three-dimensional dense diamond-like structure and produces the two new families of ternary compounds, with the formulas $A_2Hg_3Q_4$ and $A_2Hg_6Q_7$, which have Hg/Q anions with low dimensional structures. The $A_2Hg_3Q_4$ compounds consist of linear chain anions separated by alkali metal cations. The $A_2Hg_6Q_7$ compounds display unique, tunneled 3-D structures with A^+ cations residing in parallel tunnels. The anisotropic framework structure of $A_2Hg_6Q_7$ can sustain topotactic ion-exchange reactions with LiI. The presence of Li ions in the structure causes a large bathochromic shift in the optical spectrum of $Li_2Hg_6Q_7$ because of stronger interaction with the Hg/Q framework. The $A_2Hg_6Q_7$ group compounds are medium bandgap semiconductors with optical gaps in the optimum region for efficient solar energy absorption (i.e. 1.0 eV-1.5 eV) and are (a) amenable to bandgap engineering through S/Se solid solution and (b) melt processing. These new compounds have larger bandgaps than HgQ, because of the reduced dimensionality caused by the incorporation of A_2Q into the HgQ lattice. In

turn the bandgaps of the linear chain $A_2Hg_3Q_4$ compounds are higher than those of the $A_2Hg_6Q_7$ compounds, consistent with their higher Q^{2-}/Hg^{2+} ratio, lower Hg−Q connectivity, and lower dimensionality. The noncentrosymmetric structure of $A_2Hg_6Q_7$ suggests possible nonlinear optical properties.

Acknowledgment. This research was made possible with funding from NSF Grant DMR-9527347. This work made use of the SEM facilities of the Center for Electron Optics at Michigan State University. M.G.K. is an A. P. Sloan Foundation Fellow and a Camille and Henry Dreyfus Teacher Scholar.

Supporting Information Available: Tables of calculated and observed powder patterns for $K_2Hg_3Se_4$, $Cs_2Hg_3Se_4$, $Rb_2Hg_6S_7$, $Cs_2Hg_6S_7$, $Rb_2Hg_6Se_7$, and $Cs_2Hg_6Se_{1.75}S_{3.25}$, anisotropic thermal parameters for $K_2Hg_3S_4$, $K_2Hg_3Se_4$, $Cs_2Hg_3Se_4$, $K_2Hg_6S_7$, $Rb_2Hg_6S_7$, $Cs_2Hg_6S_7$, and $Cs_2Hg_6Se_7$, and bond distances and angles for $K_2Hg_3S_4$, $K_2Hg_3Se_4$, $Cs_2Hg_3Se_4$, $K_2Hg_6S_7$, $Rb_2Hg_6S_7$, $Cs_2Hg_6S_7$, and $Cs_2Hg_6Se_7$ (36 pages). See any current masthead for ordering and Internet access instructions.

JA9713486